SAND2022-0411C

Flexible Control of Synthetic Inertia in Co-Located Clusters of Inverter-Based Resources

Thad Haines
Sandia National Laboratories
Albuquerque, NM
jthaine@sandia.gov

Felipe Wilches-Bernal
Sandia National Laboratories
Albuquerque, NM
fwilche@sandia.gov

Rachid Darbali-Zamora
Sandia National Laboratories
Albuquerque, NM
rdarbal@sandia.gov

Miguel Jiménez-Aparicio
Sandia National Laboratories
Albuquerque, NM
mjimene@sandia.gov

***Abstract*—This paper uses co-located wind and photovoltaic generation, along with battery energy storage, as a single plant and introduces a method to provide a flexible synthetic inertia (SI) response based on plant-wide settings. The proposed controller accounts for variable resources and correctly adjusts device responses when an inverter-based resource (IBR) may become unavailable to provide a consistent plant level SI response. The flexible SI response is shown to adequately replace the lost synchronous inertial response from equivalent conventional generation when IBR penetration is approximately 25% in a small power system. Furthermore, it is shown that a high gain SI response provided by the combined IBR plant can reduce the rate of change of frequency magnitude over 50% from the equivalently rated conventional generation response.**

***Index Terms*—Resource Aware Synthetic Inertia, Fast Frequency Response, Inverter-Based Resource**

I. Introduction

As fossil-based generation is replaced with renewable wind and solar generation, the bulk electric power system loses the synchronous inertia response provided by physically rotating masses [1]. Synthetic inertia (SI) has been proposed as a possible control solution for declining levels of synchronous inertia [2]. The physics based kinetic-to-electrical energy conversion associated with synchronous inertia, which opposes changes in system frequency (often synonymous with rotational speed), occurs naturally in generation sources that involve rotating masses. SI is purely a power systems control concept applied to inverter-based resources (IBRs). This means generation operators must configure their equipment to provide a SI response in a similar manner as one would configure a frequency-watt or volt-VAR droop controller. This adds a level of complexity, but also allows for possible improvements as the inertial response is not tied to a physical parameter and may be controlled to further aid frequency response. However, due to the variable nature of renewable resources, extra precaution should be taken to ensure a control signal is not sent to a device that cannot physically respond.

This work is part of a larger project to allow IBRs to be flexibly controlled in similar, or better, ways than conventional generation [3]. Specifically, this work demonstrates ways to distribute the SI response among various types of co-located IBRs as if the group were a single power plant that can account for variable resource availability. The group of controlled IBRs, defined as a FlexPower plant, is similar to a virtual power plant [4] except all generating devices are co-located. While the concept of using IBRs to mimic the dynamics of conventional synchronous generation is not a new research topic [5], [6], and the strengths and shortcomings of SI (also referred to as virtual, emulated, or artificial inertia) have been discussed in various use cases [7]–[12], there has not been a focus on coordinating the SI response between distinct generation sources as this work does.

The structure of this paper is as follows: Section II describes the simulated test system and models, Section III gives an overview of SI and the basis of adaptive control, Section IV provides simulation results, and Section V offers the conclusions of this work.

II. Test System and Models

A one-line diagram of the system used in these experiments is shown in Fig. 1. The three-bus system contains a conventional generator on Bus 1, a static and switchable load on Bus 2, and a FlexPower plant consisting of a battery energy storage system (BESS), a wind turbine (WT), and a photovoltaic (PV) plant co-located on Bus 3. This simple test system was designed in Simulink to clearly show the effects of varying levels of SI response from the FlexPower plant. Further details about the device models are provided in the following subsections.

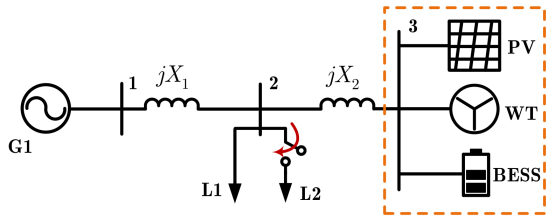

Fig. 1: One line diagram of test system with FlexPower plant on Bus 3.

A. Photovoltaic Inverter

The model used for the photovoltaic inverter was adapted from [13]. It contains an average inverter model that controls real and reactive power via pulse width modulation signals that define the direct and quadrature current injections. The PV model was rated at 40 MVA and set to curtail 5 MW to allow for SI participation. An optional irradiance profile input was set to the device's rated value of 1000 $\mathrm{W/m^2}$.

B. Battery Energy Storage System

The BESS inverter was modeled similarly to the PV, but includes a state of charge (SOC) variable that defines the amount of energy the BESS may provide as described in [14].

For short simulations that do not greatly affect the SOC, a value above or below the operating threshold was set during model initialization to define if the BESS is available to absorb or provide power. The BESS model was rated at 10 MVA and was not initially generating or absorbing any power for all simulations. This was meant to reflect an idle BESS ready to accept any dispatch signal.

C. Wind Turbine Generator

A Type-4 wind turbine model was used for the WT connected to Bus 3. The model is described and validated in [15]–[17]. Real and imaginary current injections act as the grid interface for the WT to supply real or reactive power, respectively. The WT has blade pitch control to mechanically set the generated power and also contains functionality to directly control the inverter output to allow for faster set point changes. The WT model had a rating of 60 MVA and was initially curtailing 5 MW to allow for SI participation.

D. Conventional Generator

The conventional generator G1 is a standard MATLAB 3-phase synchronous machine modeled in the dq rotor reference frame [18]. Most parameters for the model were taken from a range of typical values presented in [19]. The 300 MVA rated machine was equipped with an exciter, a governor with a droop of 5%, and was initially operating at approximately 52% capacity.

III. Synthetic Inertia

This section introduces the SI model used and describes the approach taken to provide a flexible plant SI response. It should be noted that fast frequency response (FFR) is the preferred term to describe an IBR's rapid response to system changes [1] and SI can be classified as a type of proportional FFR.

A. Generic Model

A generic SI model is depicted in Fig. 2. The input is a measured frequency signal that is passed through a derivative, low-pass filter, deadband, gain, and a limiter. The output signal from the SI model is then added to the P_{ref} of a device to increase or decrease real power output in a way that opposes frequency change. It should be noted that while S_{rated} shown in Fig. 2 may relate to the physical MVA rating of a particular device, the value is somewhat arbitrary as the overall gain block contains k, which can effectively create any gain desired.

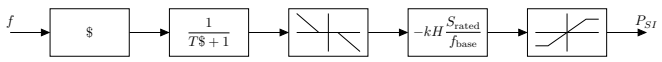

Fig. 2: Model of SI used in test system.

Standard values for the low-pass filter time constant T, frequency derivative deadband, arbitrary gain k, inertia constant H, and frequency base f_{base} are listed in Table I. S_{rated} is normally the same as the device MVA rating.

TABLE I: SI model symbols and initial parameter values.

Name	Symbol	Value	Unit
System Frequency	f	-	Hz
Laplace Variable	\$	-	sec^{-1}
Filter Time Constant	T	0.2	sec
Deadband	-	0.02	Hz/sec
Arbitrary Gain	k	10	-
Inertia Constant	H	4	sec
Device Rating	S_{rated}	-	MW
System Base Frequency	f_{base}	60	Hz

B. Adaptive Model

The proposed adaptive SI model makes use of a centralized plant controller that accepts a desired plant MVA rating S_{plant}, inertia constant H, and an arbitrary gain k as parameters. Additionally, the controller is assumed to know if a device is participating in the inertial response and any resource limitations associated with each device (e.g. SOC of a BESS, solar irradiance level of a PV plant, or wind speed of at a WT). The output of the centralized plant controller is a new S_{rated} value for each connected device's SI control shown in Fig. 2. For example, if the new S_{rated} is calculated as

$$S_{\text{rated}} = S_{\text{plant}}/N \tag{1}$$

where N is the sum of participating devices, the result would be an equal sharing (EQS) of SI response from all connected devices. If N is equal to 0, there are no devices participating in the inertial response and the controller would command all devices to not provide any SI. If a device is lacking resources, the controller may adjust the participation status of that device, which would alter the calculation of S_{rated}.

Currently, the controller is designed to allocate the SI response to each available device equally, however a cost function could be introduced to favor one device over another depending on resource availability. Additionally, the arbitrary gain k could be adjusted to provide a larger inertial response. A much larger inertial response may cause system instability or not deliver expected results due to device output limitations.

IV. Simulation Results

The simulated event in all simulations was the 10 MW load L2 on Bus 2 being connected at $t = 1$. Various scenarios were used to examine the effect of SI on rate of change of frequency (ROCOF). ROCOF is simply the slope of a line drawn between two points of a frequency response [1]. In this work, the calculation for ROCOF between arbitrary times a and b, where $a < b$, is

$$\text{ROCOF}_{a,b} = \frac{f(b) - f(a)}{t(b) - t(a)}. \tag{2}$$

Typically, ROCOF is calculated 0.5 seconds after a perturbance [1]. This work also calculates the ROCOF between $(0, 0.1)$ and $(1, 2)$ seconds after an event (equivalent to $\text{ROCOF}_{1,1.1}$ and $\text{ROCOF}_{2,3}$, respectively in (2)). These additional ROCOF calculations were chosen to capture the maximum SI response, which typically occurred 0.1 seconds

after an event, and the transition of the SI response to the conventional governor response approximately 1 second after the event. The real power contribution from each case is presented as a useful visual representation of the SI response from all participating devices. The calculation is simply

$$P_{\text{contribution}} = P - P_{t=0} \tag{3}$$

where P is a time series of real electrical power output.

A. Base Case Scenarios

To simulate a conventional generation inertial response reference, the PV, WT, and BESS connected to Bus 3 were replaced with a conventional generator, G3, with parameters similar to G1. The rating of G3 was set to 110 MVA (a sum of the MVA ratings for Bus 3 connected IBRs), its inertia constant was set to 4 seconds, and the turbine speed governor was disabled. The power contribution of both generators from this *conventional* case is shown in Fig. 3. G3 contributed a maximum of approximately 2.5 MW of inertial response while G1 contributed nearly 7 MW and also provided governor action for the rest of the simulation. This behavior of G1 was similar in all cases.

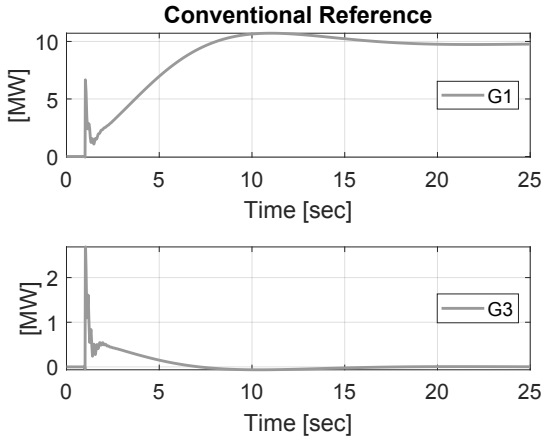

Fig. 3: Power contribution of conventional generation to a 10 MW step.

G3 was then replaced with the previously described IBRs and SI was enabled. Device SI gains were adjusted until the frequency response from a proportional response case nearly matched the conventional reference case. Power contributions from the base IBR case and proportional SI case are shown in Fig. 4. Proportional control used device MVA ratings as S_{rated} in the SI control to dictate the response magnitude. The operation of this control is visually apparent by the power contribution of the WT being larger than the PV, and both being larger than the BESS response magnitude. Without SI control, the WT power fluctuated down after the load step, while the other devices did not respond. When SI control was enabled, the WT was marginally slower to respond than both the PV or BESS. It should be noted that the conventional reference signal is plotted for **reference only** as G3 is not present in the system when IBRs are connected.

System frequency from these tests is shown in Fig. 5. The loss of synchronous inertia in the base IBR case increased the ROCOF magnitude and slightly lowered the frequency nadir. These results also show that SI can be used to replace the lost synchronous inertia.

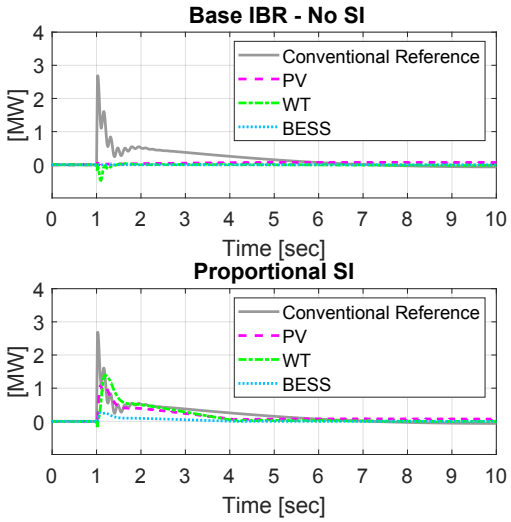

Fig. 4: Power contributions from the base IBR case and proportional SI case.

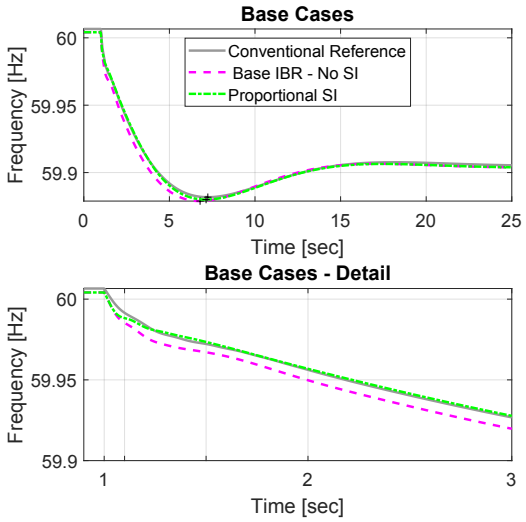

Fig. 5: Frequency response of base case scenarios. The unlabeled x axis markings in the detail plot represent 1.1 and 1.5, which are used in ROCOF calculations.

Table II presents three calculated ROCOF values from each control case. The $\text{ROCOF}_{1,1.1}$ magnitude increased by approximately 38 mHz/sec, or 25%, when IBRs were introduced (coincidentally, this is equivalent to roughly 25% IBR penetration). This first ROCOF value slightly improved when proportional SI was employed, though did not exactly match the conventional reference case. $\text{ROCOF}_{1,1.5}$ values between the proportional case and conventional reference were similar, while the base IBR case was slightly faster due to the longer SI response. $\text{ROCOF}_{2,3}$ was approximately the same for all cases as this value is most heavily influenced by G1's governor response which is consistent throughout all simulations.

TABLE II: ROCOF from base cases presented in mHz/sec.

	$\text{ROCOF}_{1,1.1}$	$\text{ROCOF}_{1,1.5}$	$\text{ROCOF}_{2,3}$
Conventional Reference	-150.60	-68.69	-29.43
Base IBR - No SI	-188.36	-74.07	-30.03
Proportional SI	-158.80	-61.29	-29.15

B. Individual Response Scenarios

The simulations in this section allocated all SI response to a single device. Fig. 6 shows that the power contribution from all IBRs were similar to one another and slightly larger and longer in duration than the conventional reference response.

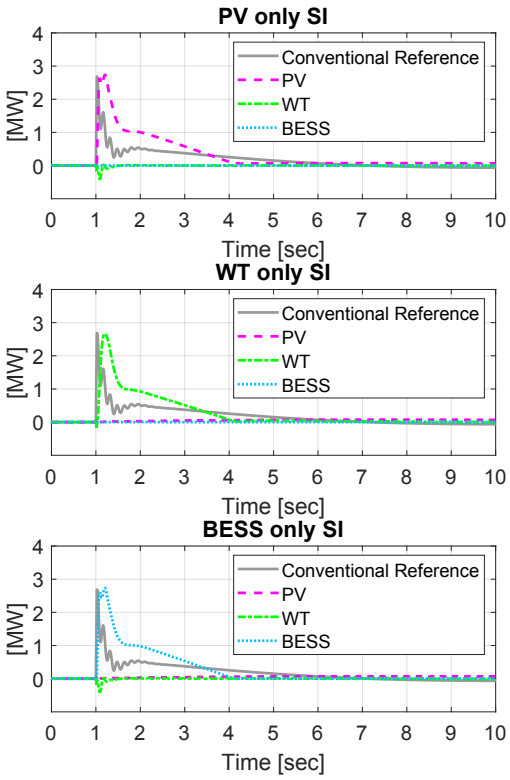

Fig. 6: Power contributions from the single SI response cases.

Fig. 7 shows the frequency response from all single device cases. Generally, the IBRs deliver a very similar SI response. Table III presents the calculated ROCOF values for all time periods of interest. The WT only response is approximately 20 mHz/sec larger in magnitude than other cases during the first time period due to a slightly slower SI response.

TABLE III: ROCOF from single device cases presented in mHz/sec.

	$\text{ROCOF}_{1,1.1}$	$\text{ROCOF}_{1,1.5}$	$\text{ROCOF}_{2,3}$
Conventional Reference	-150.60	-68.69	-29.43
PV only SI	-149.96	-61.29	-29.14
WT only SI	-167.99	-61.29	-29.16
BESS only SI	-149.44	-61.27	-29.14

C. Equal Sharing with Resource Awareness Scenarios

The results in this section are from enabling all resources to participate in the SI response and allowing the plant controller to set SI gains such that each device receives the same signal. Additionally, resource awareness (RA) was enabled in one

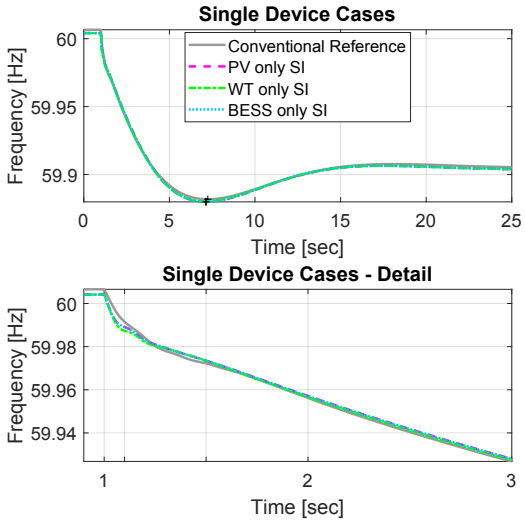

Fig. 7: Frequency response of single device SI response scenarios.

case where the BESS SOC was set below its operational threshold. Fig. 8 shows that with RA enabled, the EQS control method functions properly increases the PV and WT output to make up for the BESS not responding. Fig. 9 shows that frequency response in all EQS cases was similar. While Table IV shows that ROCOF was only slightly worse when the BESS output was limited, it also shows that RA can properly dispatch the SI response to other plant devices if one is unavailable.

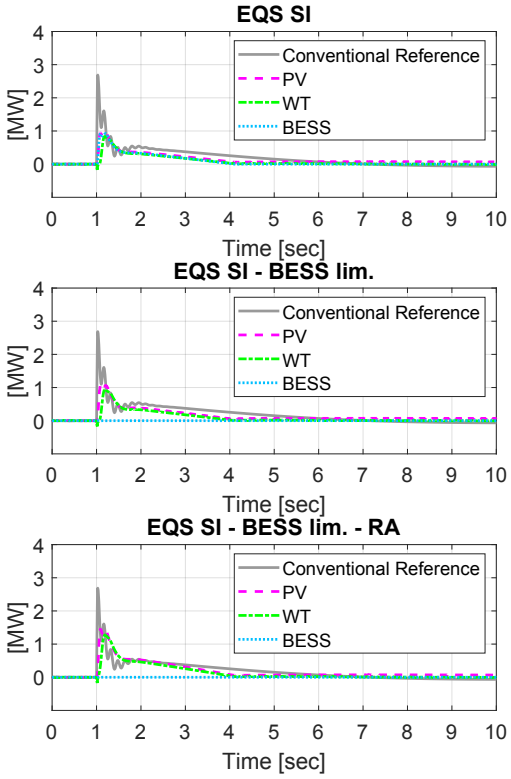

Fig. 8: Power contributions from equal sharing and RA SI response cases. The BESS was resource limited in two cases to show how the RA control method would adjust the other device's response to accommodate.

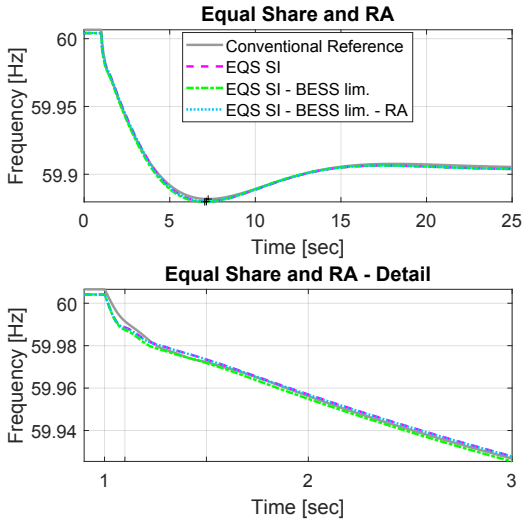

Fig. 9: Frequency response of equal share and RA SI response scenarios.

TABLE IV: ROCOF from equal sharing cases presented in mHz/sec.

	$\mathrm{ROCOF}_{1,1.1}$	$\mathrm{ROCOF}_{1,1.5}$	$\mathrm{ROCOF}_{2,3}$
Conventional Reference	-150.60	-68.69	-29.43
EQS SI	-155.00	-61.29	-29.15
EQS SI - BESS lim.	-167.02	-64.60	-29.48
EQS SI - BESS lim. - RA	-158.10	-61.30	-29.15

D. High Gain Scenarios

For the high gain scenarios, k in the SI model (Fig. 2) was changed from 10 to 80, and the SI response was distributed equally among all devices in one case, and to only the PV and BESS in another. The power contributions from all IBRs are larger than the conventional reference in Fig. 10, which resulted in a reduction of $\mathrm{ROCOF}_{1,1.1}$ by about 65 mHz/sec (57%) and a reduction of approximately 30 mHz/sec (57%) in $\mathrm{ROCOF}_{1,1.5}$. These values were calculated based on Table V. It is worth noting that ROCOF values are very similar between the two high SI gain scenarios despite different levels of device participation.

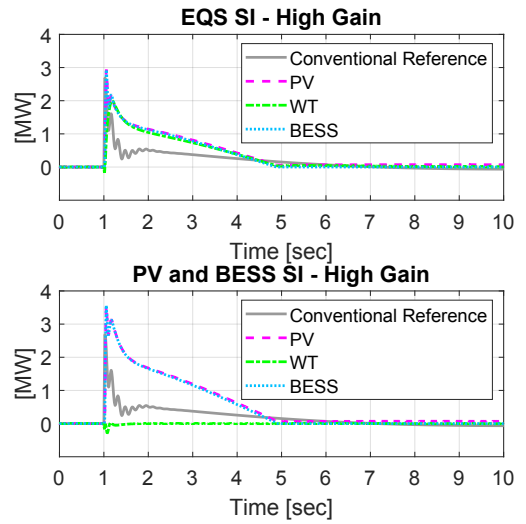

Fig. 10: Power contributions from high gain SI response cases.

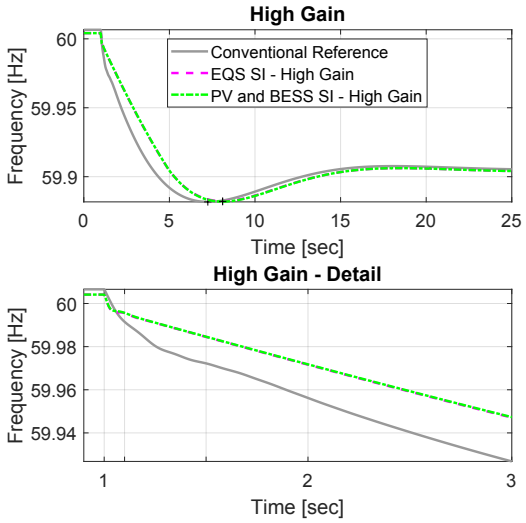

Fig. 11: Frequency response of high gain SI response scenarios.

TABLE V: ROCOF from high gain cases presented in mHz/sec.

	$\mathrm{ROCOF}_{1,1.1}$	$\mathrm{ROCOF}_{1,1.5}$	$\mathrm{ROCOF}_{2,3}$
Conventional Reference	-150.60	-68.69	-29.43
EQS SI - High Gain	-85.89	-39.29	-24.52
PV and BESS SI - High Gain	-84.69	-39.07	-24.46

V. Conclusion

This paper introduced a flexible SI modeling approach to allow clusters of IBRs to replace the synchronous inertia response provided by a traditional generator. Various distributions of SI participation among co-located PV, WT, and BESS were explored. Results from this study showed that SI response from different types of IBRs can be very similar if a controlled device has enough available capacity to respond. If a device's variable resources prevent SI participation, the resource-aware controller can allocate other available devices to make up the shortfall so the plant-level SI response is consistent. Other simulation results showed how increased SI gains may reduce ROCOF magnitude over 50% from what an equivalent synchronous inertial response may provide. Further development of the SI controller may involve incorporating a cost function into the inertial response allocation process to allow for a more economically influenced dispatch of resources.

VI. Acknowledgment

The paper describes objective technical results and analysis. Any subjective views or opinions that might be expressed in the paper do not necessarily represent the views of the U.S. Department of Energy or the United States Government.

Sandia National Laboratories is a multimission laboratory managed and operated by National and Engineering Solutions of Sandia, LLC., a wholly owned subsidiary of Honeywell International, Inc., for the U.S. Department of Energy's National Nuclear Security Administration under contract DE-NA0003525.

This research was supported by The U.S. Department of Energy's Grid Modernization Laboratory Consortium program.

REFERENCES

[1] NERC Inverter-Based Resource Performance Task Force, "Fast frequency response concepts and bulk power system reliability needs," Tech. Rep., 2020.

[2] P. Denhold, T. Mai, R. W. Kenyon, B. Kroposki, and M. O'Malley, "Inertia and the power grid: A guide without the spin," National Renewable Energy Laboratory, Tech. Rep., 2020.

[3] NREL. NREL Researchers Study Synergistic Value Streams in Hybrid Power Plants. [Online]. Available: https://www.nrel.gov/news/program/2021/flexpower.html

[4] J. Johnson, J. Flicker, A. Castillo, C. Hansen, M. El-Khatib, D. Schoenwald, M. A. Smith, R. Graves, J. Henry, T. Hutchins, J. Stamp, D. Hart, A. Chavez, M. Burnett, J. Tabarez, C. Glatter, B. Xie, A. P. Meliopoulos, P. Huynh, H. Zhu, and K. Davis, "Design and evaluation of a secure virtual power plant," Sandia National Laboratory, Tech. Rep., 2017.

[5] H.-P. Beck and R. Hesse, "Virtual synchronous machine," in *2007 9th International Conference on Electrical Power Quality and Utilisation*, 2007, pp. 1–6.

[6] Q.-C. Zhong and G. Weiss, "Synchronverters: Inverters that mimic synchronous generators," *IEEE Transactions on Industrial Electronics*, vol. 58, no. 4, pp. 1259–1267, 2011.

[7] F. Gonzalez-Longatt, E. Chikuni, and E. Rashayi, "Effects of the synthetic inertia from wind power on the total system inertia after a frequency disturbance," in *2013 IEEE International Conference on Industrial Technology (ICIT)*, 2013, pp. 826–832.

[8] E. Shoubaki, S. Essakiappan, M. Manjrekar, and J. Enslin, "Synthetic inertia for bess integrated on the dc-link of grid-tied pv inverters," in *2017 IEEE 8th International Symposium on Power Electronics for Distributed Generation Systems (PEDG)*, 2017, pp. 1–5.

[9] R. J. Concepcion, F. Wilches-Bernal, and R. H. Byrne, "Effects of communication latency and availability on synthetic inertia," in *2017 IEEE Power Energy Society Innovative Smart Grid Technologies Conference (ISGT)*, 2017, pp. 1–5.

[10] J. Gollenstede, L. Beushausen, R. Benger, H. P. Beck, M. Schael, W. Kruschel, T. Ulbrich, and S. Schmies, "Design of a high-performance battery converter system for providing synthetic inertia at distribution network level," in *2018 20th European Conference on Power Electronics and Applications (EPE'18 ECCE Europe)*, 2018, pp. P.1–P.10.

[11] B. K. Poolla, D. Groß, and F. Dörfler, "Placement and implementation of grid-forming and grid-following virtual inertia and fast frequency response," *IEEE Transactions on Power Systems*, vol. 34, no. 4, pp. 3035–3046, 2019.

[12] F. Wilches-Bernal, J. Wold, and W. H. Balliet, "A method for correcting frequency estimates for synthetic inertia control," *IEEE Access*, vol. 8, pp. 229 141–229 151, 2020.

[13] A. Yazdani and R. Iravani, *Two-Level, Three-Phase Voltage-Sourced Converter*. Wiley-IEEE Press, 2010.

[14] P. Pourbeik, S. E. Williams, J. Weber, J. Sanchez-Gasca, J. Senthil, S. Huang, and K. Bolton, "Modeling and dynamic behavior of battery energy storage: A simple model for large-scale time-domain stability studies," *IEEE Electrification Magazine*, vol. 3, no. 3, pp. 47–51, 2015.

[15] M. Shao, N. Miller, J. Sanchez-Gasca, and J. MacDowell, "Modeling of GE Wind Turbine-Generator for Grid Studies," General Electric International, Inc., Schenectady, NY, Tech. Rep. Version 4.6, Mar. 2013.

[16] N. Miller, J. MacDowell, G. Chmiel, R. Konopinski, D. Gautam, G. Laughter, and D. Hagen, "Coordinated voltage control for multiple wind plants in eastern wyoming: Analysis and field experience," in *2012 IEEE Power Electronics and Machines in Wind Applications*. IEEE, 2012, pp. 1–8.

[17] J. M. MacDowell, K. Clark, N. W. Miller, and J. J. Sanchez-Gasca, "Validation of ge wind plant models for system planning simulations," in *2011 IEEE Power and Energy Society General Meeting*. IEEE, 2011, pp. 1–8.

[18] The MathWorks, Inc. Synchronous Machine. [Online]. Available: https://www.mathworks.com/help/physmod/sps/ug/synchronous-machine.html?searchHighlight=Synchronous%20Machine&s_tid=srchtitle_Synchronous%20Machine_1

[19] P. Kundur, *Power System Stability and Control*. New York, NY: McGraw-Hill, 1994.